Displacement damage stabilization by hydrogen presence under simultaneous W ion damaging and D ion exposure

S. Markelj[a], T. Schwarz-Selinger[b], M. Pečovnik[a], A. Založnik[a,1],

M. Kelemen[a,c], I. Čadež[a], J. Bauer[b], P. Pelicon[a], W. Chromiński[d], L. Ciupinski[d]

[a]*Jožef Stefan Institute, Jamova cesta 39, 1000 Ljubljana, Slovenia*

[b]*Max-Planck-Institut für Plasmaphysik, Boltzmannstrasse 2, D-85748 Garching, Germany*

[c]*Jožef Stefan International Postgraduate School, Jamova cesta 39, 1000 Ljubljana, Slovenia*

[d]*Warsaw University of Technology Faculty of Materials Science and Engineering, Wołoska 141, Warsaw, Poland*

Abstract

Polycrystalline tungsten (W) samples were simultaneously irradiated by 10.8 MeV W ions and exposed to 300 eV deuterium (D) ions at different temperatures ranging from 450 K to 1000 K. After the simultaneous W ion irradiation and D ion exposure the samples were additionally exposed to low energy D ions at 450 K in order to populate all the defects created beforehand. The amount of damage created was evaluated by measuring D depth profiles and D thermal desorption spectra. Results are compared with data obtained in a sequential experiment where samples were first irradiated by 10.8 MeV W ions and only afterwards exposed to 300 eV D ions at 450 K to populate the created defects. At 450 K we observe a two times higher maximum D concentration for the simultaneous case as compared with the sequential case. At 600 K and 800 K the ratio between simultaneous and sequential decreases to about 1.6 and 1.2, respectively, and increases again to a factor of two at 1000 K. We attribute this dependence on temperature to the change in the concentration of mobile and trapped D during the simultaneous exposures, which is in line with theoretical calculations predicting that trapped D in a vacancy prevents vacancy annihilation with self-interstitials.

Keywords: tungsten, deuterium retention, displacement damage, NRA, TDS, damage stabilization

[*]Corresponding author: sabina.markelj@ijs.si

[1] Current affiliation: Center for Energy Research, University of California San Diego, 9500 Gilman Drive, La Jolla, CA 92093-0417, USA

1. Introduction

In a future thermonuclear device such as DEMO the wall material will be irradiated by 14 MeV neutrons produced in the D-T nuclear reaction and at the same time exposed to a high flux of ions and neutrals of hydrogen isotopes as well as helium. The most suitable materials for plasma-facing components is tungsten (W) or advanced tungsten alloys. Due to safety of operation and fuel efficiency, tritium retention in a neutron-damaged wall and other plasma-facing components is a significant issue. In order to study the influence of neutron irradiation of materials on fuel retention, high-energy W ions produced by MV accelerators are used to produce displacement damage [1] which mimic the damage created by neutrons very well, while also providing faster damage rates [2]. The important differences between ion and neutron damaging which still remain are that neutrons cause transmutations of the material constituents and create damage throughout the material while ions create displacement damage within the ion range.

To the authors' best knowledge in all experiments where fuel retention in displacement-damaged tungsten was studied by ion or plasma loading, the high energy W ion damaging and exposure to deuterium was performed sequentially: first the displacement damage was created in a hydrogen free material and only then hydrogen exposure began. However, in real fusion devices creation of displacement damage and hydrogen isotope irradiation will take place simultaneously. This difference in the conditions at which damage is created, meaning with or without the presence of hydrogen isotopes, is important when studying fuel retention. Some theoretical calculations show that the presence of hydrogen as an interstitial atom can lower the vacancy formation energy [3] or that hydrogen clusters can prevent a vacancy from recombining with the neighboring crowdion-type self-interstitial-atom [4]. Moreover it was shown experimentally by positron annihilation spectroscopy that vacancy-hydrogen complexes have a higher barrier associated with their migration in metals like tantalum and niobium [5] compared to hydrogen free vacancies.

Recently, we performed first experiments where W samples were simultaneously damaged by high energy W ions and exposed to D atoms [6]. By comparing simultaneous W ion irradiation and D atom exposure to sequential W ion irradiation and D atom exposure, it was shown that the presence of deuterium has an influence on fuel retention and consequently on defect stabilization [6, 7]. In that case the sub-eV energy D atoms, need to overcome a large energy barrier to migrate from the surface into the bulk [8, 9] to be able to further diffuse in the bulk and populate defects produced by the W irradiation. This barrier prevented us from performing simultaneous damaging/atom loading studies bellow 600 K since the penetration depth of D atoms is strongly reduced at lower temperatures. For instance, at 450 K exposure temperature D atoms penetrated only 200 nm deep even after a few days of exposure [9]. As DFT calculations [10] show, vacancies have a de-trapping energy bellow 1.5 eV. As a consequence, they are not occupied during the 600 K exposure, which further means the effect of

the presence of D on their production could not be seen in [6, 7]. On the contrary, ions with energy above eV directly penetrate into the bulk and diffuse through bulk and consequently populate defects in the material also at lower temperatures. As a consequence, in the ion exposure case, the vacancies can be occupied because of lower exposure temperature and hence we should be able to see the effects of the presence of D on vacancy production. In addition, due to the direct penetration of ions into the bulk, processes at the surface are not the rate limiting ones as is the case for atom exposure with sub eV energy [7]. Therefore, the concentration of mobile hydrogen atoms that diffuse through interstitial positions in the tungsten lattice is different for the two cases as a function of temperature.

Here we present results of simultaneous exposure studies where polycrystalline tungsten samples (grain size 10-50 μm) were simultaneously irradiated by high energy W ions and loaded by low-energy D ions at four different temperatures ranging from 450 K to 1000 K. In order to determine the density of the created traps in the material, the samples were additionally exposed to low-energy D ions after simultaneous damaging and loading. The deuterium depth profiles were measured by nuclear reaction analysis (NRA) using the $D(^3He,p)^4He$ reaction and the release kinetics of D were analyzed by thermal desorption spectroscopy (TDS). Results are compared with those obtained when samples were submitted to sequential W ion irradiation and D ion exposure. In addition, from a comparison with the previous experimental series with D atoms conclusions about the influence of retained D on damage stabilization will be drawn.

2. Experiment

2.1 Experimental set-up and characterization of the ECR ion gun

Some experimental results and detailed description of the INSIBA setup at Jožef Stefan Institute (JSI) Slovenia, that allows creation of displacement damage by implanting high energy ions at a given sample temperature, exposure of the samples to a well-controlled flux of atomic deuterium and measurements of deuterium depth profiles in situ can be found in previous publications [6, 11]. Details on the experimental setup as used for the present measurements are given in the next section. Here we restrict ourselves to describing mainly the upgrades with respect to the low energy D-ion implantation. Instead of the hydrogen atom source described in [11] a commercial electron cyclotron resonance (ECR) ion gun was used in this study (Tectra Gen II http://www.tectra.de/sputter.html, energy range 25 eV – 5 keV). The ion gun uses a filament-less ion source based on a microwave plasma discharge. Microwave radiation (2.45 GHz) is coupled via a coaxial waveguide into a plasma

chamber. The intense oscillating electric fields cause the gas breakdown and a stable plasma discharge to be formed. A multipole magnetic field around the chamber further enhances the plasma density via the electron cyclotron resonance effect. Ions are extracted from the plasma using simple two grid single-hole extraction optics. The use of microwaves to sustain the plasma allows ions to be extracted at very low energies without the plasma collapsing.

The ion gun was characterized before we started with the experiment. It was mounted on the dual beam experiment Bombardino at Max-Planck-Institut für Plasmaphysik (IPP), Garching, Germany at the position of the Duoplasmatron ion source [12]. By mounting the Peabody flange and an adaptor the exit of the ion gun was 4.5 cm away from the Einzel lens. Behind the Einzel lens there were x/y steerers and a Faraday cup with a 5 mm diameter orifice to measure the total ion current. We performed ion gun calibration measurements at 3 kV accelerating voltage for which stable plasma conditions were achieved. The forwarded microwave power was kept constant and the gas flow was varied. The actual pressure in the plasma chamber could not be measured. Gas was introduced to the ion gun through a thin long tube connected to the plasma chamber and was pumped out into the vacuum chamber through a 3 mm dimeter ion gun exit orifice. The driving pressure was regulated by a leak valve. The increase of the pressure in the vacuum chamber depends on the pumping speed and the gas flow through the ion gun. In the following text we refer for all measurements to the pressure increase in the vacuum chamber as measured by an ion gauge. The plasma started to be stable at a nitrogen equivalent pressure of 4.2×10^{-5} mbar delivering a measurable current of 20 nA on the Faraday cup. We attained a maximum ion current of 300 nA at 1.5×10^{-4} mbar. Increasing the pressure up to 7×10^{-4} mbar leads to a linear decrease of the ion current down to 180 nA.

A mass analysis was performed in order to determine which ion species are dominant for the ion source when working with deuterium gas. The 60° bending magnet placed after the x/y steerers enabled us to make a mass analysis of the beam. Due to the Lorenz force the ions travel along a circular trajectory. One can perform a mass (m) analysis of the ion beam by changing the magnetic field B at a fixed radius R and fixed energy of the ions E: $m=(RB)^2/2E$. We ran a mass scan at 3 kV accelerating voltage at several fixed pressures and measured the ion current on the sample placed in the Bombardino chamber as a function of current through the magnet coils. When feeding D_2 gas to the gun we obtained three peaks at certain values of magnetic field that were assigned to masses 2 amu/e, 4 amu/e and 6 amu/e which are attributed to D^+, D_2^+ and D_3^+ ions. The ion species distribution as a function of the pressure in the chamber is shown in Fig 1. One can observe that the ion flux on average consists of 93% of D_3^+ ions. The contribution of D^+ ions is almost independent of the pressure and D_2^+ decreases with the increase of the pressure. At a pressure of 1.5×10^{4} mbar where the maximum current was obtained we get 93% of D_3^+ ions, 4.6% of D_2^+ ions and 2% of D^+ ions. At 2.4×10^{-4} mbar the beam consists of 96% of D_3^+ ions, 1% of D_2^+ ions and 3% of D^+ ions. We believe that the ion distribution depends mainly on the pressure inside the plasma chamber and is

representative also for other applied acceleration voltages, i.e. energies. We performed also a retarding field analysis by applying a positive bias on the repelling electrode of the Faraday cup at 0.9 kV ion accelerating voltage. By this we obtained the information of the energy distribution for a 900 eV ion energy deuterium beam. The full width at half maximum of the measured ion current was 25 eV at 1.5×10^{-4} mbar pressure increasing to 34 eV at 2.9×10^{-4} mbar.

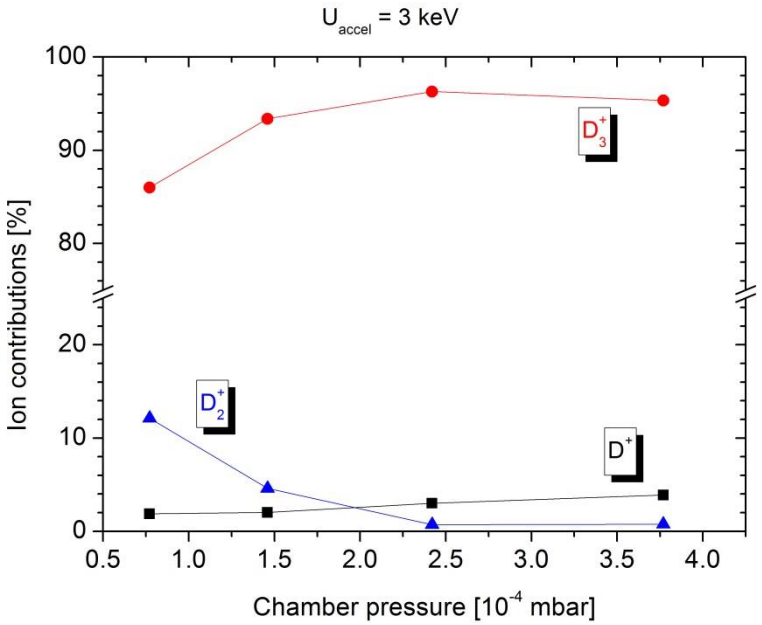

Figure 1: The contribution of individual ions (D^+, D_2^+ and D_3^+) to the total ion current as a function of vacuum chamber pressure.

After the described performance measurements, the ion gun was mounted in the INSIBA chamber at JSI where simultaneous and sequential W ion damaging and D ion exposures were performed. The ion gun was positioned at a 51^o angle with respect to the sample surface normal and the probing ion beam from the 2 MV Tandem accelerator. The schematic drawing of the set-up is shown in Fig. 2. A bias of 100 V is applied at the sample to suppress the secondary electrons and to allow for accurate ion current measurement. An acceleration voltage of 1 kV was chosen for the later exposures. The energy of the majority of the ions is then 300 eV/D and for this ion energy the maximum transferred energy [13] is below the threshold for displacement damage in tungsten [14]. We, therefore, do not expect to produce additional damage to the tungsten lattice by the D ion beam. According to the manufacturer manual the ion beam is very broad especially at low acceleration voltage. Moreover, the distance from the ion gun exit to the sample surface had to be rather large, being 170 mm, due to geometrical constraints. For this reason, the ion flux at the probing ion beam position of the sample was very low. In order to increase the ion flux on the sample an Einzel lens was designed in house specifically for this purpose and was mounted between the ion gun and the sample. The Einzel lens was mounted 5 mm from the exit of the ion gun plasma chamber. The lens has a standard configuration A/D=1 where the length of the middle cylinder (A) is equal to the inner diameter of the

cylinder (D), being 26 mm. Maximum current on the sample was achieved at 760 V on the Einzel lens for 1 kV ion beam acceleration voltage. The maximum ion current on the sample was reached in the INSIBA vacuum chamber at the same pressure of 1.5×10^{-4} mbar as in the calibration measurements. For this reason, we believe that the pumping speeds of the two vacuum systems are similar and we can directly apply the characteristics of the ion gun obtained from the above calibration measurements also for the exposure conditions in the INSIBA set-up. The ion current directly measured on the sample was 27±2 µA. The lateral ion flux distribution was determined exposing a plasma-deposited diamond like amorphous hydrogenated carbon thin film (a-C:H) on a Si wafer to the beam and measuring the erosion crater by ellipsometry. The 71 nm thick a-C:H film was exposed to the D ion beam for one hour at 600 K. The average ion current measured on the sample was 26±1 µA. By taking the erosion yield for 300 eV D ions at elevated temperature to be 0.1 removed C per incoming D [15] the observed erosion depth of 21 nm converts with the carbon density of 9×10^{28} C/m^2 [16] to a maximum ion flux of 5×10^{18} D/m^{2}s. The flux distribution as obtained from the ellipsometry measurement is shown in Fig. 3. One can observe that the ion beam from the ion gun is rather well focused with dimensions of about 2.5 mm full width at half maximum in the vertical direction but with a long tail and 4 mm in size in the horizontal direction with a nonzero offset. The larger horizontal dimension is because the ion beam hits the sample under 51^o with respect to the surface normal. In Fig. 3 we also marked the position of the ion beam from the accelerator (damaging W beam and analysing ^{3}He beam). At this location the mean D ion flux is $(1.3\pm0.4)\times10^{18}$ D/m^{2}s. As can be seen the two beams were rather poorly aligned even though we put efforts to mechanically align the ion gun and the Einzel lens with respect to the sample centre where the probing beam from the accelerator hits the sample. An explanation for this mismatch is a possible misalignment between the Einzel lens, the extraction orifice and the actual plasma distribution inside the ion source.

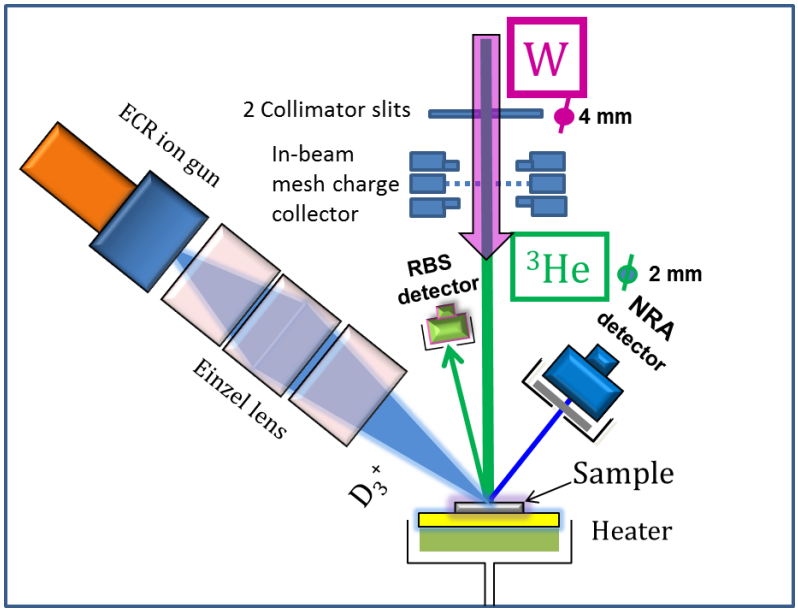

Figure 2: Schematic picture of the setup for the simultaneous W ion irradiation and D ion exposure, where the ECR ions source and the Einzel lens are positioned at 51^o angle with respect to the probing ^{3}He or W ion beam. The NRA detector and RBS detectors are also shown positioned at a scattering angle of 135^o and 165^o degrees with respect to the probing beam, respectively.

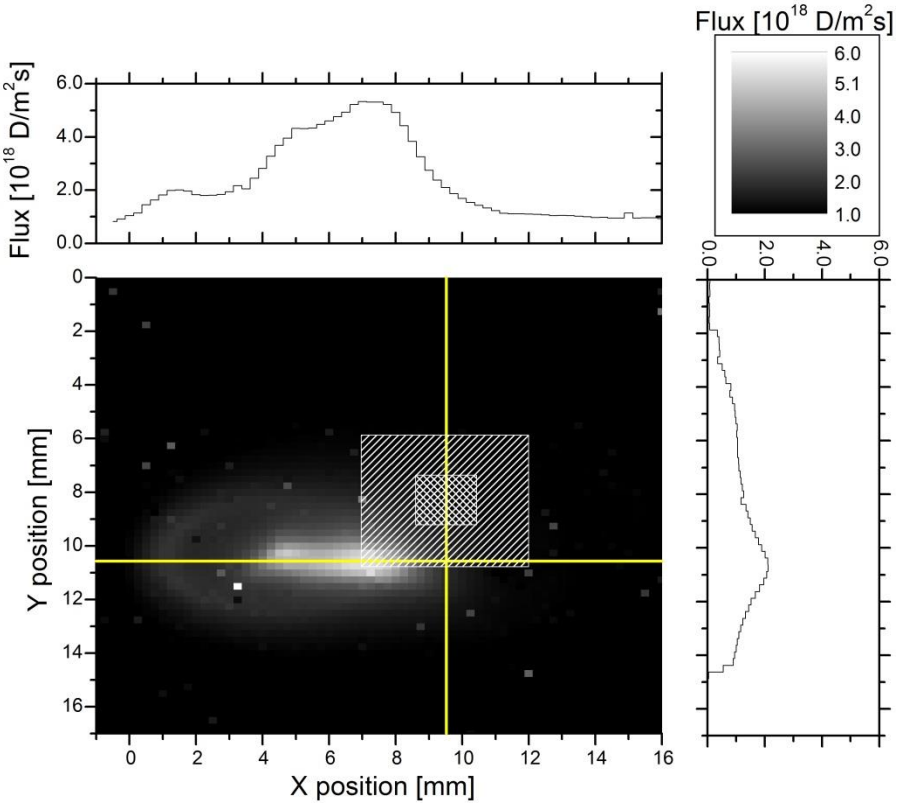

Figure 3: 2D and lateral ion beam profile as determined by ellipsometry from an a-C:H film after D-ion exposure at 600 K for one hour with 1 kV accelerating voltage and 0.76 kV voltage applied to the Einzel lens. The crossed straight lines indicate at which positions the lateral and vertical ion beam profiles are plotted. The erosion depth was converted with an erosion yield of 0.1 C/D and a carbon density of 9×10^{28} C/m^2. *The dashed squares indicate the position of the probing ^{3}He (small square) and W beam (large square).*

2.2 Sequential and simultaneous W ion irradiation and D ion exposure

The sample preparation and experimental details for simultaneous and sequential W ion irradiation and D-ion exposure are similar to the case of simultaneous W ion irradiation and D atom exposure described in detail in Ref. [6].

In the present experiments we have again used polycrystalline 99.997 wt.% hot-rolled tungsten samples manufactured by Plansee, 12x15 mm^2 in size and 0.8 mm thick. Grains were

elongated in the rolling direction being parallel to the surface. The surfaces were mechanically polished down to 5 μm grit and subsequently electro-polished in 1.5% NaOH solution to a mirror-like finish. In order to reduce the density of natural defects present in the as received material, the samples were heated for 2 min in vacuum at 2000 K for re-crystallization after polishing. This procedure reduces the intrinsic defects density and enlarges the grain size to 10 - 50 μm. Reducing the defect density in the samples decreases D retention in the bulk, thereby allowing better interpretation of thermal desorption spectra of D from the damaged layer and enables its clearer identification by transmission electron microscopy (TEM). The use of the same manufacturing batch enables us to compare these results to our previous results performed with D atoms [6].

In the present configuration the INSIBA set-up enables us to simultaneously expose a sample to a high energy W ion beam to induce displacement damage and to low-energy deuterium ions from the ECR ion gun to expose and decorate the produced defects. The sample was mounted on a holder with a computer-controlled ceramic heater, which enabled us to heat the sample up to 1100 K during the W ion irradiation and D ion exposure (see Fig. 2). The sample was fastened to the heater by two Ta clamps and temperature was measured by three thermocouples (TC). One TC was mounted in the heater and the other two on the sample surface attached by the Ta clamps, one at the top and one at the bottom of the sample. The typical temperature difference between TCs in the heater and the sample was 50 K, with the heater being hotter. The difference between the TCs on the sample was about 10 K. The higher value, from TCs attached to the sample, is used for the sample temperature in the following. To induce displacement damage, tungsten samples were irradiated by 10.8 MeV W^{6+} ions perpendicularly with respect to the sample surface for four hours at certain sample temperature. The beam size was defined by a pair of collimator slits in the beam line, see fig. 2. The real beam size was checked by irradiating a polished graphite sample by 10.8 MeV W ions. By visual inspection it was found that the beam is square shaped with a 5 mm long edge. The W ion current was first set to the desired value by measuring it on the ion mesh charge collector with 77.4% geometrical transmission [17]. The ion mesh charge collector was then retracted in order not to have a mesh-print on the sample. The stability of the current was checked by inserting the mesh every 20-30 minutes. The ion current was stable within ±10% yielding an uncertainty of the total ion fluence of about 10% for all irradiated samples. After the end of the measurement the ion current was re-checked by measuring the ion current directly on the sample with a bias of 100 V applied to it. The corresponding W ion irradiation current on the sample was 1.6 nA and the irradiation time was four hours yielding a W ion fluence of $(1.0\pm0.15)\times10^{18}$ W/m^2 on the irradiated 5x5 mm^2 square irradiation spot. The displacement damage profile as calculated by SRIM [18] is peak shaped and extends down to 1.2 μm. With a fluence of 1.0×10^{18} W/m^2 we create a damage dose of 0.35 dpa_{KP} (Kinchin-Pease calculation, 90 eV displacement damage energy [14], evaluating the "vacancy.txt" output [18, 19]) at the peak maximum yielding a displacement rate of 2.4×10^{-5} dpa/s.

In the following we will report on two different experimental series performed with this configuration of the INSIBA set-up. In the first series W ion damaging was performed alone for four hours at a specific temperature. The low energy D ion exposure was only performed afterwards. We name this sequential W ion irradiation and D ion exposure, shortly 'sequential W-D exposure'. The W ion irradiation was performed at five different temperatures 300 K, 450 K, 600 K, 800 K and 1000 K. After the W irradiation each sample was exposed to D ions with energy of 300 eV/D for 39 hours at 450 K, in order to populate the traps created during the damaging. The current of the D ion beam collected at the sample was measured all the time and it was for all exposure cases 26±2 μA on average. The corresponding D ion flux averaged over the W ion beam spot was $(1.3 \pm 0.1)\times10^{18}$ D/m^{2}s as was determined from the ion flux density profile shown in Fig. 3. The D ion fluence after 39 h of exposure is 1.8×10^{23} D/m^2. After W ion damaging and D ion exposure D depth profiles were derived by NRA for all samples in-situ in the INSIBA chamber at JSI and also ex-situ at IPP. The lateral D distribution was measured in addition ex-situ by NRA at IPP, to check the homogeneity of D exposure. After the ex-situ NRA analysis TDS was performed.

In the second experimental series both high energy W ion irradiation and exposure to low energy D ions were performed simultaneously. We name this experiment simultaneous W ion irradiation and D ion exposure or in short 'simultaneous W/D exposure'. The W and D energies were identical as before. The experiment lasted again four hours at a specific temperature, yielding the same final damaged dose of 0.35 dpa_{KP} as in the sequential case and a D ion fluence of 1.9×10^{22} D/m^2. The experiment was performed at four temperatures 450 K, 600 K, 800 K and 1000 K. In order to populate the created defects and to be able to compare with the sequential experiment the samples were additionally exposed to D ions with energy of 300 eV/D at 450 K for 39 h yielding the same fluence of 1.8×10^{23}D/m^2 at the analysing beam position as in the sequential case. We name this simultaneous W ion irradiation and D-ion exposure with additional D-ion exposure in short 'simultaneous W/D-D exposure'. The samples simultaneously W/D exposed were analysed by NRA in-situ at JSI right after the four hours W/D exposure and again later during and after the additional D exposure of 39 h. The lateral D distribution was measured ex-situ by NRA at IPP. Finally, TDS was performed after the ex-situ NRA analysis. A second batch of samples was prepared in an identical way by simultaneous W/D-D exposure and sent for TEM analysis to Faculty of Materials Science and Engineering, Warsaw.

2.3 NRA and TDS analysis

The NRA analyses were performed in-situ in the INSIBA set-up at JSI, Fig. 2, at six ^{3}He ion beam energies from 700 keV to 4300 keV to probe the sample from the surface up to a depth of 7 μm.

We used the same collected charge for all six energies, corresponding to 14.9 μC ion dose for He^+ (9.3×10^{13} He ions) for the four lower energies and 7.45 μC ion dose for He^{2+} (4.65×10^{13} He ions) for the two highest energies. The protons from the D(^{3}He,p)α nuclear reaction were detected using a 1500 μm thick partially depleted Passivated Planar Silicon (PIPS) detector. The NRA detector was mounted at 135^o scattering angle with a solid angle of 26.7 msr. A 24 μm Al absorber was placed in front of it, to stop the backscattered ^{3}He ions. The second PIPS detector with 300 μm thick depletion region was placed at 165^o scattering angle for detecting the Rutherford backscattered projectile particles (RBS detector). The ^{3}He beam was collimated by a circular aperture with a diameter of 2 mm. The diameter of the analysing beam for NRA was smaller than the diameter of the W ion irradiated area (5 mm square), to make sure that we analysed the damaged area only. The D depth profile analysis typically took place right after the exposure or the latest the next day which is after about 16h. We did not observe outgassing from the samples, which we believe is due to the fact that we exposed damaged samples where de-trapping energies are high, as will be seen in the following.

Due to the large inhomogeneity of the deuterium ion flux profile, shown in Fig. 3, we checked the inhomogeneity of deuterium retention at the RKS set-up at IPP ex-situ on all samples. The set-up is described in detail in [19]. We measured the proton signal at single ^{3}He energy of 2.4 MeV with 5 μC ion dose along the vertical and horizontal axis of the sample. We chose this energy since the beam penetrates deep enough to give information about D retention in the whole damaged zone. The scan was made with 1 mm beam size in steps of 1 mm. The high energy protons from the nuclear reaction between ^{3}He and D were analysed using a thick, large angle PIPS detector at a scattering angle of 135° and a solid angle of 75 msr. The proton signal along the longer axis is shown in Fig. 4 for three sequential W-D and two simultaneous W/D-D samples irradiated at the indicated temperatures. The samples were mounted on a holder that enables NRA analysis of five samples at the same time. Measurements were performed along the longer Y axis of samples, the same Y axis as on figure 3, in the centre of the shorter X axis. We can observe that the proton signal increases substantially in the middle of the sample which is the area where W ion damaging was performed and is approximately 5 mm wide. This is in good agreement with the spot size obtained previously on the graphite sample. The proton signal increases slightly at the right part of the beam spot indicating that the D beam is not homogeneous and retention depends on the D ion flux and fluence. Based on this we estimated from Fig. 3 the mean D ion flux within the 1 mm ^{3}He beam size at the edge of the W ion damaging area to be $(1.9 \pm 0.1)\times10^{18}$ D/m^{2}s, yielding a fluence of 2.7×10^{23} D/m^2 for the 39 h exposure. The flux at that position is almost 50% larger than the average ion flux.

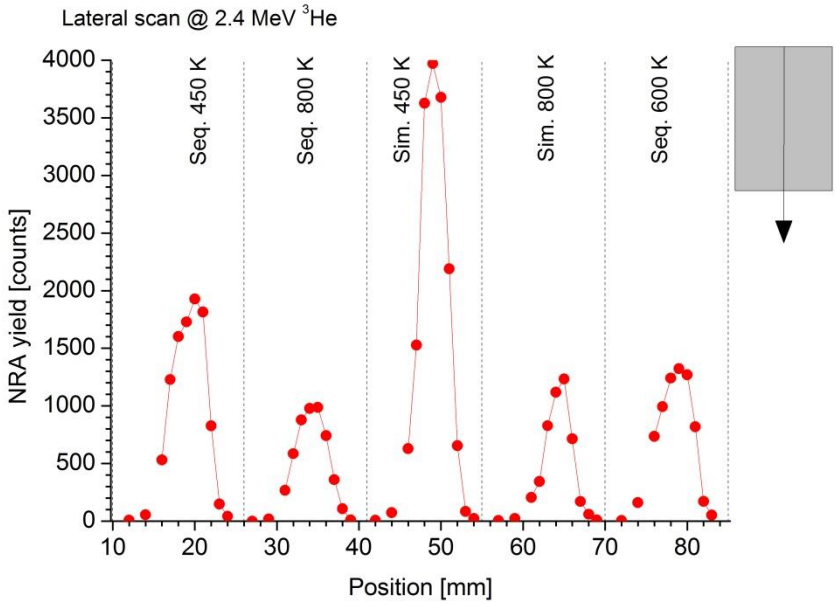

Figure 4: Proton signal at 2.4 MeV ^{3}He energy as measured ex-situ in the middle of the sample, along the vertical dimension of the 15 mm long samples indicated in the sketch. Abscise denotes the position on the sample holder and vertical dotted lines mark the border between the samples. On holder position 10-25 mm we show data for sample sequential W-D at 450K, on holder position 25-40 mm data for sequential W-D at 800 K, from 40 to 55 mm data for simultaneously W/D-D exposed sample at 450K, from 55 to 70 mm data for simultaneous W/D-D at 800 K and from holder position 70 to 85 mm we show data for sequential W-D at 600 K.

At the position where the maximum of the proton counts at 2.4 MeV ^{3}He energy was measured we also performed a D depth profile analysis (NRA max). Eight different ^{3}He energies ranging from 500 keV to 4.5 MeV were used, probing the sample down to 7.4 μm depth. The D concentration within the near-surface layer at depths down to about 0.3 μm was determined by analysing the emitted α particles with a surface barrier detector at the laboratory scattering angle of 102° for ^{3}He energies of 500 keV, 690 keV and 800 KeV. A rectangular slit is placed in front of the α detector which reduces the solid angle to 9.16 msr but increases resolution. A nominal pre-set charge of 10 μC was accumulated for each ^{3}He energy (6.2×10^{19} He/m^2).

To check the performance of the detectors, to calibrate the energy scale and to minimize the absolute scatter in D areal densities as calibration sample an amorphous-deuterated carbon thin film (*a*-C:D), of known D content was measured for each energy. Calibration measurements were performed on both set-ups at JSI and IPP with the same *a*-C:D film. All deuterium depth profiles were obtained by simultaneous deconvolution of proton and alpha spectra measured at different energies using the SIMNRA [20] and NRADC [21] software. Differential cross section by Wielunska et al. [22] and total cross section by Besenbacher and Möller [23] were used.

After the NRA measurement the retained D amount of the specimens was measured by TDS also named temperature programmed desorption (TPD) in the quartz tube of the TESS device at IPP [24]. The samples were heated up to a sample temperature of 1010 K with an oven heating ramp of 3 K/min. The maximum temperature of 1010 K is high enough to ensure desorption of all retained D from the samples [25]. The temperature response of the samples to the linear oven temperature ramp was calibrated in independent experiments by a thermocouple spot-welded to a tungsten sample of identical size and surface finish. The desorbed gases were measured with a Pfeiffer/Inficon DMM 422 quadrupole mass spectrometer (QMS). The following 15 mass channels were recorded: m/z = 1, 2, 3, 4, 12, 14, 16, 17, 18, 19, 20, 28, 32, 40, and 44. Mass channels above 4 showed no significant release of deuterium containing species. Background contributions were determined in a preceding and a subsequent temperature ramp without sample or with an outgassed sample in the heating zone, respectively. Measurements showed only negligible contributions in mass channel 4 and contributions in the percentage range for mass channel 3 which was subtracted in the latter case. For the quantitative analysis the QMS signal for D_2 was calibrated after each temperature ramp with a Laco leak bottle with a flow of 1.22×10^{14} D_2/s and a stated absolute accuracy of 4.6%. The calibration factor for HD was experimentally determined by flowing D_2 and HD gas through an orifice of know size from a calibrated volume into the QMS vessel [26]. Based on the pressure recording of a spinning rotor gauge the calibration factor in HD molecules per measured QMS counts was 66% of the one derived for D_2 molecules. Contribution of HD on the total D desorption was 20% on average. The accuracy for the absolute amount for D is determined by the stated accuracy of the leak valve.

2.4 TEM analysis

TEM observations were performed on thin lamellas cut with standard focused ion beam (FIB) procedures from irradiated areas of simultaneous W/D-D exposed samples. A Hitachi NB5500 SEM/FIB microscope with Ga^+ ion source was used for this purpose. During TEM analysis the region of observation was tilted to the closest <001> type zone axis and then a series of four different two-beam conditions were set to obtain a full view of the dislocation network viewed under different imaging conditions. In this paper images with excited **g** =$(\bar{1}10)$ will be presented. All TEM imaging was performed on a JEOL JEM 1200EXII microscope operated at 120 kV accelerating voltage.

3. Results

3.1 D depth profiles

a) Sequential W-D exposure

We will first present results obtained on sequential W-D samples prepared at five different temperatures of 300 K, 450 K, 600 K, 800 K and 1000 K. The deuterium depth profiles were measured by NRA in-situ in the INSIBA set up with a 2 mm wide beam in the centre of the W irradiation spot. For the 450 K and 300 K case we measured the deuterium depth profile during the D ion exposure (21 h and 25 h for 450 K and after 18 h for 300 K) in order to study the dynamics, i.e. to check how much D ion fluence is needed to populate the whole damaged zone. After 18 h (fluence of 0.84×10^{23} D/m^2) for the 300 K case and after 25 h (fluence of 1.4×10^{23} D/m^2) for the 450 K case the total D amount was already 81% and 82% of the final D amount obtained after total 39 h exposure, respectively. Since almost doubling the D ion fluence increased the total amount by less than 20% we believe that 39 h of D-ion exposure corresponding to a D fluence of 1.8×10^{23} D/m^2 was largely enough to populate all the defects in the damaged zone. This should also hold for W ion irradiation at higher temperatures where the trap concentration is even lower, as will be explained in the next paragraph. We want to stress here that it is crucial to know how much D fluence is needed to populate the defects in the whole damaged layer by D since the transport of D is dominated by trapping and de-trapping at the defects [8]. If the D fluence is too low and the defects are not completely populated by D throughout the whole damaging depth, the comparison of the depth profiles and TDS spectra is not straightforward. Namely, as it was shown in [9] that additional peaks could appear in the TDS spectra that are not due to trapping in a defect but because of D diffusion deeper into the bulk and then back to the surface during thermal desorption. Exposing such type of samples to too high fluences however does not influence the result as retention is only limited to the damaged zone. Retention in the bulk is negligible due to the initial recrystallization at 2000 K.

The final D depth profiles measured after D ion exposure are shown in Fig. 5. We show only the D depth profiles measured at IPP at the location of the maximum proton yield (NRA max) from Fig. 4 where the flux was $(1.9 \pm 0.1)\times10^{18}$ D/m^{2}s and the fluence was 2.7×10^{23} D/m^2 after 39 h of exposure. Comparing these depth profiles with the ones measured in the centre of the damaging spot at JSI (not shown), both measurements are in good agreement and are within the error bars when comparing both the D concentration depth distribution and the maximum D concentrations. Hence, the slightly different flux and fluence for the two experimental series have no effect on the further interpretation. In all cases we see an increased D retention down to a depth of 1.2 µm, which is in nice agreement with the SRIM calculation of the depth of the created damage also shown in Fig. 5. However, the D depth profile is more or less homogeneous in this area and does not follow the calculated SRIM damage depth profile. This was already observed in e.g, [27, 28] and was explained by the fact that D concentration saturation sets in at about 0.1-0.2 dpa_{KP} damage dose. In our case the damage dose is above this level down to 1 µm and for this reason the D depth profile flattens. The maximum D concentration in the middle of the damaged zone decreases with increase of the damaging temperature from 1.4 at.% for damaging at 300 K down to 0.25 at.% for damaging at 1000 K. This in total is an 82%

reduction of D retention. Because the decoration of the defects was done at the same temperature for all samples we can infer from this maximum D concentration that the concentration of traps induced by the W ion irradiation reduced in the same manner. Decreasing D retention with increasing irradiation temperature was already observed in the case of the sequential experiment with D-atom loading at 600 K and was attributed to defect evolution and partial annealing at higher temperatures [7]. However, besides this similarity, the maximum D concentration is almost by a factor of three higher in the present case of D ion exposure as compared to the atom loading. We think that this is due to lower exposure temperature in the present case where traps with lower de-trapping energy than 1.83 eV [7] can be populated. Moreover, due to direct ion implantation into the bulk the concentration of mobile atoms is much higher than in the 0.28 eV atom exposure case.

For reference we show in figure 5 also the D depth profile of an undamaged recrystallized W sample. This sample was not damaged by W ions but only exposed to 300 eV/D deuterium ions for 39 h. The near surface areal density attains 2×10^{19} D/m^2 and the bulk concentration is 4×10^{-4} at.%. The latter we attribute to intrinsic defects remaining after the 2000 K annealing. High near surface concentration is also observed in the damaged samples attaining surface areal density of 2-3$\times10^{19}$ D/m^2 on top of the D retention which is due to defects from W ion damaging. This amount of surface areal density we attribute to deuterium adsorbed on the surface at chemisorption sites at this low exposure temperature as was already explained and shown in [11].

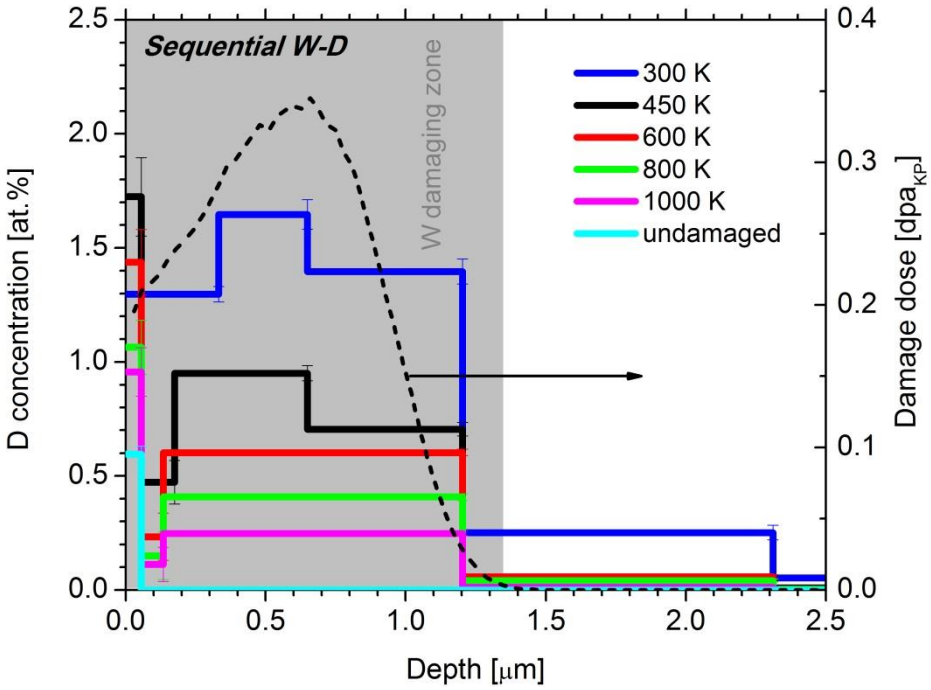

Figure 5: D depth profiles measured at the position of maximum proton counts of Fig. 4 on samples with sequential W-D exposure at different temperatures. After the W ion irradiation the samples were exposed additinally to D ions at 450 K, energy 300 eV/D and flux (1.9 ± 0.1)×10^{18} D/m^{2}s yielding a

fluence of 2.7×10^{23} D/m^2 after 39h of exposure. The D depth profile for an undamaged W sample exposed to D ions at 450 K is also shown. The black dashed line shows a SRIM calculation of the damage depth profile with damage dose values on the right Y scale.

b) Simultaneous W/D exposure

In order to study the defect evolution in the presence of D, simultaneous W/D exposure was conducted. The experiment was performed at four temperatures: 450 K, 600 K, 800 K and 1000 K. The D depth profiles obtained after this four hours of simultaneous W/D exposure at the centre of the W irradiation area are shown in Fig. 6a. Already after this short time a significant D retention is observed at 450 K and the D managed to diffuse almost through the whole damaged zone. The D concentration is 1.4 at.% from the surface down to 0.4 μm depth and then decreases to 0.5 at.% down to 1 μm. For the exposure at 600 K the maximum D concentration is only 0.2-0.3 at.% and it decreases even further by an order of magnitude for exposures at 800 K and 1000 K. In all cases D was present throughout the whole damaged region at the end of the simultaneous experiment. The drastic decrease in D concentration is mostly due to the significant thermal de-trapping of atoms at higher temperatures.

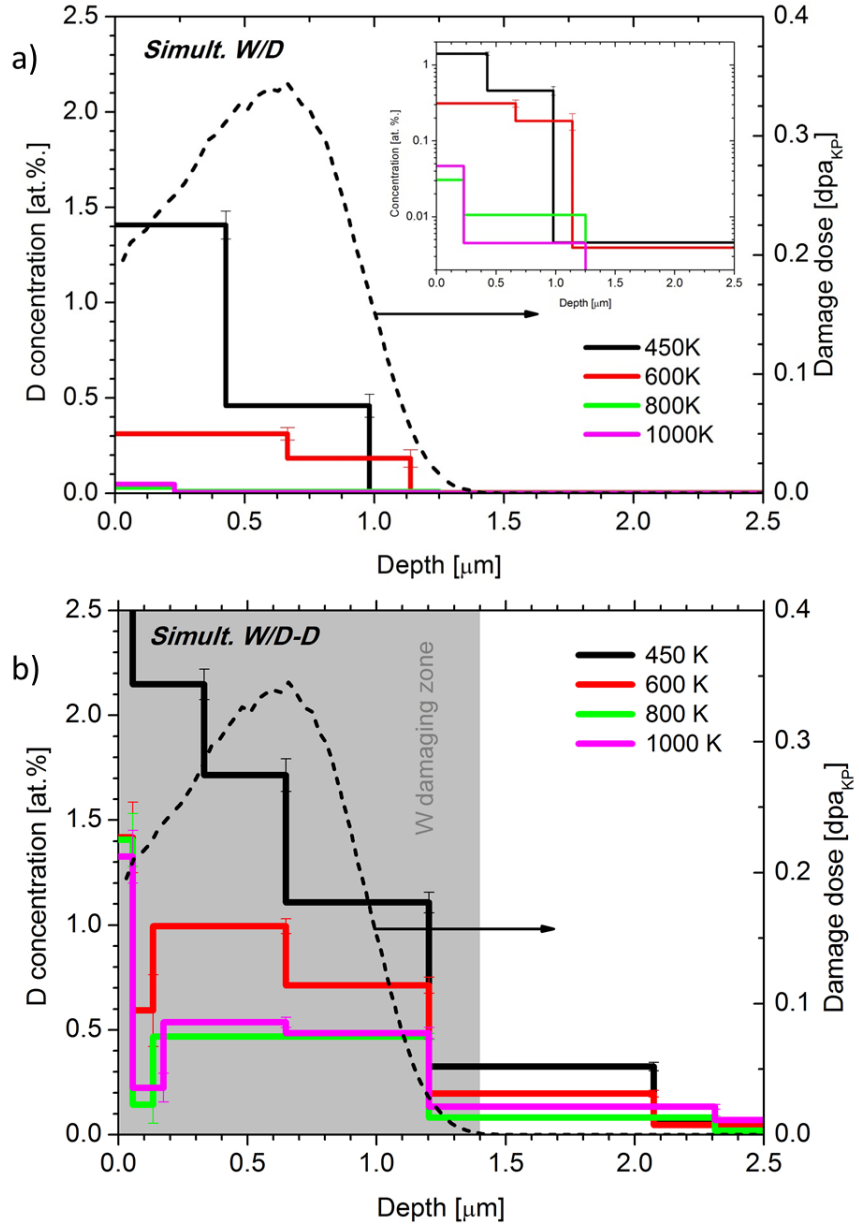

Figure 6: Simultaneous W ion damaging and D ion exposure a) D depth profiles obtained after four hours. Depth profile was measured in the centre of the damaging area. The D ion fluence was 1.9×10^{22} D/m^2 and the final damage dose was 0.35 dpa$_{KP}$. The inserted graph shows the same data with the ordinate in logarithmic scale. b) D depth profiles of the same samples after the additional D ion exposure for 39 h (ion energy 300 eV/D and ion fluence 2.7×10^{23} D/m^2). Depth profile measured at the position of maximum proton signal (NRA max). The black dashed line shows a SRIM calculation of the damage depth profile with damage dose values on the right Y scale.

c) Additional D decoration W/D-D

In order to populate the created defects and to be able to compare with the sequential results the samples were additionally exposed to D ions with the same energy of 300 eV/D at 450 K for 39 h. D depth profiles for the sample position where the maximum proton signal (NRA max) was measured

are shown in Fig. 6b. The D ion flux at this position was $(1.9 \pm 0.1)\times10^{18}$ D/m^{2}s, yielding a D ion fluence of 2.7×10^{23} D/m^2. Two main observations can be made based in Fig 6b: D retention increased for all samples in the damaged zone after this additional D exposure and the D concentration in the damaged zone is still highest at the lowest damaging temperature. However, there are more distinct differences observed. First, significant D retention is observed for the 800 K and 1000 K sample. Both show a maximum concentration of 0.5 at.%. From the post-annealing experiments of self-damaged tungsten [27, 29] one could expect a continuous reduction in D concentration as the defects evolve and anneal. However, this is obviously not the case if hydrogen is present during damaging. On the contrary, the maximum D concentration stabilizes above 800 K. A similar behaviour was found for the simultaneous W/D-D exposures with D atoms [6]. Second, the D concentration for the experiment at 450 K is much more peaked towards the surface after this additional loading than before. The onset of this surface peaking was already visible during the simultaneous W/D where higher trapped D atom concentration near the surface was observed, Fig. 6a. We also get a D concentration profile that peaks towards the surface in the case of the 600 K experiment but flat D depth profiles for the 800 K and 1000 K experiments. If we compare the average values of D concentrations down to 0.5 um depth we get 1.95 at.% for 450 K, 1 at.% for 600 K and 0.5 at.% for 800 K and 1000 K. There is again also an increase of the D concentration at the surface which we attribute to surface adsorption of deuterium at 450 K. This is not observed after the simultaneous W/D since the exposure took place at higher temperatures where the D surface areal density decreases [30]. and moreover with the measurement at JSI the surface resolution is not so good due to not measuring α particles from the reaction that enable better near surface D determination, as explained above.

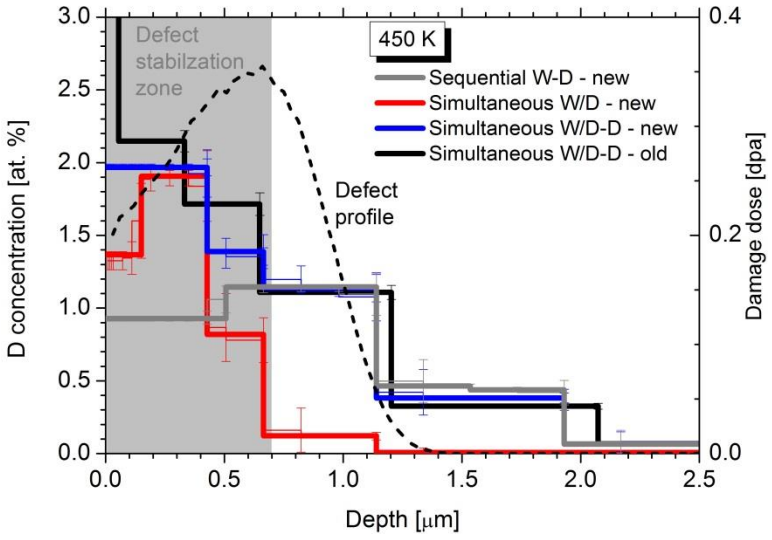

Fig. 7: D depth profiles for the repetition of the simultaneous W/D and W/D-D and sequential W-D exposure at 450 K with laterally more homogeneous D flux distribution. The results are also compared to the depth profile shown in Fig. 6b. The dashed line shows again the displacement damage calculated with SRIM.

For the case of 450 K substrate temperature we repeated the sequential W-D and simultaneous W/D-D experiment. The D depth profiles are shown in Fig. 7 (labeled 'new'). For these experiments the ion source was replaced by an identical model with larger insertion depth but without Einzel Lens in front. The exit orifice of the ECR plasma chamber was only 4.2 cm away from the sample surface. As a consequence, the beam profile was more homogenous across the sample still reaching a flux of $(1.4 \pm 0.2)\times10^{18}$ D/m^{2}s at the central position. In Fig. 7 we show the D depth profile after the simultaneous W/D exposure and the D depth profile obtained after simultaneous W/D-D exposure. It can be clearly seen that in this case after 4h the D atoms populated the defects down to 0.7 µm (red line). In that region we observe after the additional D ion exposure a factor of two higher D concentration for the simultaneous experiment (blue line) as compared to the sequential (grey line). Beyond the marked area that we named "defect stabilization zone", as will be explained bellow, the D concentration for the two cases agree with each other. For comparison of the reproducibility of the experiment we show also the D depth profile for the 450 K simultaneous W/D-D shown in Fig. 6b (black line, labelled old). We conclude from these independent measurements that the effect of D presence on defect stabilization is clearly visible and pronounced in the region where D was present during the damaging.

3.2 TDS and total D amounts

The comparison of D thermal desorption spectra for the sequential W-D exposure and the simultaneous W/D-D exposure is shown in Fig. 8. The total D desorption for each experiment is shown and is derived by summing up the D contributions from D_2 ad HD. The TDS spectra look very similar to the one obtained on a sample damaged at 300 K and exposed to D ions at 450 K, also shown. This is a representative spectrum for damaging at room temperature typically performed also in other laboratories [29, 31, 32].

We observe two prominent D desorption peaks for all cases, one at 600 K and the second one at 750 K. The first peak is dominant for experiments at 450 K and 600 K but becomes the same height as the second peak in the case of the 800 K experiment. With the increase of the W irradiation temperature both peaks decrease for the simultaneous and the sequential case. For 450 K the low and the high temperature D desorption peaks are higher by a factor of 1.8 and 1.5 in the simultaneous experiment as compared with the sequential one, respectively. In the 600 K case the D desorption peaks are both by a factor of 1.3 higher for the simultaneous case. This shows that the presence of D influences the defect annihilation or stabilization on defects in both peaks similarly. The D desorption

peaks are more or less of the same height for the simultaneous and sequential exposure at 800 K meaning that there is hardly any effect of the presence of D during damaging. At 1000 K the D desorption peaks are again higher for the simultaneous experiment by a factor of 1.4 as compared to the sequential case. The peaks shape and height stay similar for the spectrum obtained for the simultaneous experiment at 800 K whereas they are lower for the sequential sample.

The D desorption spectrum for undamaged recrystallized W sample is also shown in Fig. 8. We observe a major peak at 580 K and small contribution also at higher temperatures for this sample .

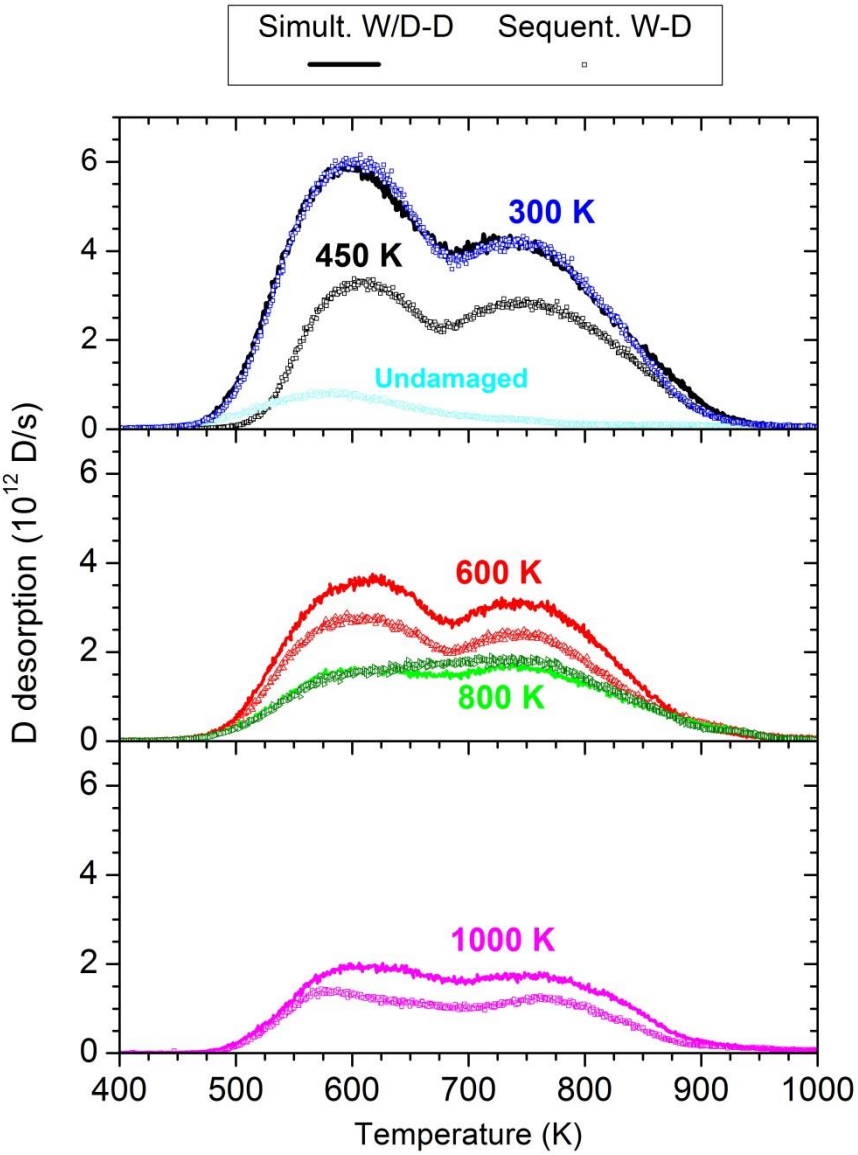

Figure 8: D desorption spectra derived by summing up the D contributions from D_2 and HD for sequential W-D exposure (open symbols) and simultaneous W/D-D exposure (lines) as a function of sample temperature. We also show a spectrum (blue squares) for the sample that was damaged at 300 K and for an undamaged sample (cyan line) both exposed to D ions at 450 K. Samples were heated with 3 K/min ramp up to 1000 K.

Finally, shown in Fig 9, we also compare the total amount of D retention for the sequential W-D and simultaneous W/D-D exposure as measured by NRA and TDS measurements. We show two sets of data for the NRA as obtained from the measurement at JSI (denoted "NRA centre") and at IPP (denoted "NRA max"). In the first case we measured the D depth profile in the centre of the damaging spot right after the exposure in situ and in the second case we measured it at the location of the maximum proton signal. We also show the D total amount for the undamaged reference W sample, exposed to D ions for 39 h. The total D amount for the reference sample is 2.2×10^{19} D/m^2 which is a factor of 30 smaller as compared to the total amounts obtained on the damaged samples. Therefore, the contribution from the area that was not irradiated by W ion beam is minor and we can directly compare the total D amounts per damaged area obtained from the samples where the sequential or simultaneous experiment was performed. Good agreement between NRA and TDS is observed, which shows the reliability of both independent quantifications. This is especially the case for the sequential experiment where the agreement is within the error bars. For the sequential experiment retention measured at the maximum proton peak (NRA max) is still within the error bars but always slightly higher than the JSI measurement (NRA centre). The difference is significantly larger for the simultaneous case where we have an increase of about 30% of D retention for the measurement at the maximum proton signal compared to the centre position. The difference could be due to the local D-ion flux. Namely, in the D ion exposure case the flux determines the concentration of mobile D atoms in the lattice, also called solute atoms. Larger concentration of mobile atoms increases the speed of filling the available traps and consequently increases stabilization of the defects. On the contrary, there is good agreement between TDS that averages over the damaged area (5 mm square) and the 2 mm diameter NRA spot measured in the centre of the damaged area. Both average over the damaged area and hence the fact that they coincide shows the reliability of both quantifications. The D retention decreases with temperature of the experiment for the sequential case and is below the simultaneous case for all temperatures. D retention for the simultaneous case decreases with temperature up to 800 K, but slightly increases for 1000 K. The D total amount for simultaneous W/D-D exposure at 450 K is about a factor of two higher as compared with the sequential experiment. For the 600 K case the difference is smaller, being a factor of 1.5, and it decreases down to 1.2 for 800 K. The difference increases at 1000 K where we have a factor of 2.5 between simultaneous and sequential experiment.

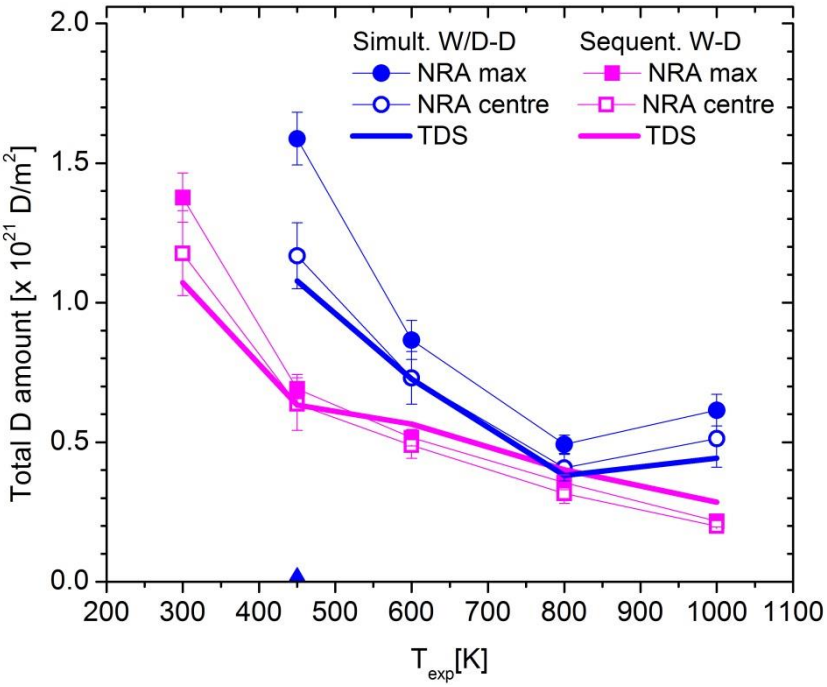

Figure 9: Total D amount for sequential W-D exposure and simultaneous W/D-D exposure as obtained by TDS (line) and NRA (symbols). The latter was performed at the position of maximum proton signal, "NRA max", as well as in the centre of the damaging area, "NRA centre". The blue triangle shows the D total amount of an undamaged W sample for reference.

3.3 TEM results

Fig. 10 shows a series of TEM images visually comparing the dislocation structures as seen in the samples that were simultaneously W ion irradiated and D ion exposed. A clear correlation between irradiation temperature and defects arrangement can be seen. In the sample treated at 450 K (fig. 10a) dislocation tangles with almost uniform distribution of dislocation lines can be noticed. Tangles seem to be formed spontaneously without any preferred crystallographic plane. Tilting the sample revealed that using different diffraction vectors for imaging changes the appearance of the tangles. This observation implies the participation of dislocations with different Burgers vectors in the observed structures. Fig. 10b depicts dislocation structures in the sample irradiated at 600 K. The appearance of dislocations arrangements appears to be more ordered than in the previous sample. Here, rather short segments of dislocation lines are distributed homogenously but no tangling can be observed. Exemplary some dislocation lines are marked with white circles. Similarly, to the previous sample, the tilting experiments reveal the presence of dislocations with various Burgers vectors. When comparing the dislocation density (Fig. 11) of these two specimens, calculated as described in [27], one can see that there is no significant difference between them. This indicates that the annealing temperature of 600 K does not annihilate these defects but only cause their spatial rearrangement. The

next image (Fig. 10c) is taken from the specimen irradiated at 800 K. Even at the first glance, one can see significant changes when comparing to the previous samples. Isolated segments of dislocation lines (marked with black circles) can be observed which suggests annihilation of defects. Dislocations density measurements (Fig. 11) confirm this statement: The density drops by 8% from 1.67×10^{14} m^{-2} to 1.55×10^{14} m^{-2}. The process of dislocation annihilation continues at higher temperature. The image of the sample irradiated at 1000K (Fig. 10d) shows only several isolated dislocation lines which can be noticed mostly due to strain contours close to them. A few examples are marked with circles. The dislocation density in this sample is with 0.94×10^{14} cm^{-2} significantly lower than in the previous three.

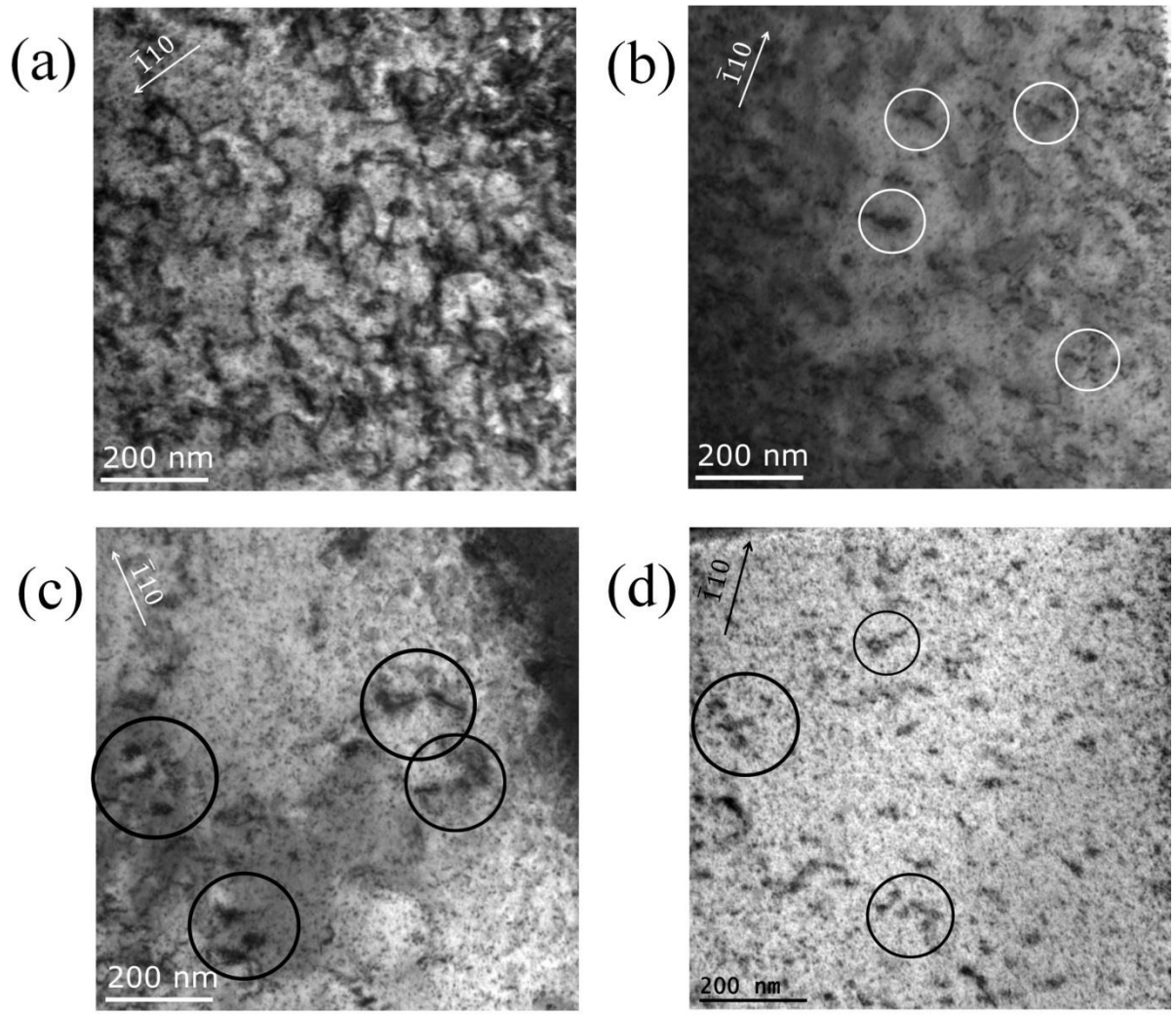

Fig. 10: TEM images of dislocation structures observed in samples simultaneously W/D-D exposed at temperatures of: (a) 450 K (b) 600 K (c) 800 K and (d) 1000 K. Circles indicate examples of discussed dislocations to separate them from FIB artifacts, which are the tiny black dots.

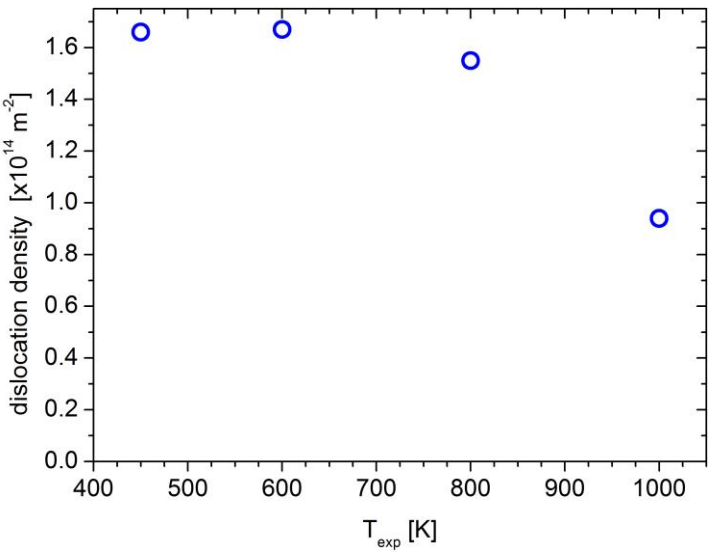

Fig.11: Dislocation densities calculated from TEM images for different simultaneous W/D-D exposure temperatures.

4. Discussion

To clearly show the difference between sequential W-D and simultaneous W/D-D exposure and to check the effect of the presence of D on damage production, we compare in Fig. 12 the local D atom concentrations derived from the D depth profiles shown in figures 5 and 6b for sequential W-D and simultaneous W/D-D exposure, respectively. In general total amounts cannot be compared between different experiments that differ e.g. in W ion energy and hence in different damaging depths or in different D fluences and hence different penetration depths. However, the average or maximum D atom concentration within the damaging zone can be directly compared without any data manipulation. It can also be used as value that is expected for the displacement damage neutrons will cause in a future fusion reactor. Therefore, we have chosen this quantity for the following discussion.

We first want to discuss the observations derived for the sequential W-D exposure. In this case the average value of D concentration in the damage zone was taken as the depth profile is rather flat. We can observe in figure 12 that in this case of sequential W-D exposure the D concentration is decreasing almost linearly with the increase of the W irradiation temperature starting already at 300 K. It is important to note that there is a significant drop of D concentration when damaging at 300 or 450 K in this sequential experiment. No such drop was observed in the case of the annealing of the defects after damaging at 300 K temperature [27, 29, 32]. At such low temperatures the vacancies are not mobile yet. For this reason, we believe that the decrease in D retention in the present case is due to higher mobility of self-interstitial atoms [33], which are mobile at these temperatures and are available during the cascade to annihilate with vacancies. When heating samples after damaging at

300 K self-interstitials are not available anymore since they diffuse to the surface or grain boundaries or form lines or loops already during the damaging and there is no change when the annealing of this structure is performed afterwards. This observation additionally confirms our results with the atoms, namely that W ion irradiation at elevated temperature or 'dynamic annealing' as called in [32] shows different behavior of defect evolution with temperature [6] as compared with damaging at room temperature and post-annealing. For comparison we added in figure 12 also the data of Ogorodnikova et al. [32] where 'dynamic annealing' was performed. The agreement with the present data is good considering that in Ogorodnikova et al. plasma exposures were performed at 470 K with ion energy of 20 eV/D and a fluence of 6×10^{24} D/m^2. Simmonds et al. [34] also performed ion damaging at elevated temperatures, however their stepped depth profiles in the damaged zone indicate that the damaged layer was not completely saturated by D and direct comparison of maximum D concentration is not possible. Namely, when samples are damaged at 300 K with a damage dose above 0.2 dpa typical D concentrations in the damaged zone are between 1.8 at.% [19, 28] and 1.2 at.% [32] for plasma exposures at temperatures between 300 K and 470 K, respectively. Their value of 0.8 at.% for 383 K exposure temperature is substantially lower.

In the following we want to compare the values of the sequential case to the ones obtained after simultaneous W/D-D exposure. Since it was clearly shown in figure 7 that the defect stabilization takes place only in the zone where deuterium is present during the four hours of simultaneous W/D we will compare the final values after the additional D exposure obtained only in that region and not the average value over the whole damaging depth. This effect of the presence of D during damaging is most prominent for the 450 K and 600 K case where high D concentrations are obtained in the first 400 nm or 600 nm, respectively, as can be seen in figure 6a. The mean D concentration obtained for the 450 K simultaneous W/D-D exposure in the first 0.5 μm depth for the two depth profiles shown in figs. 6b and 7 is 1.95 at.%. In the case of 600 K we took the maximum D concentration obtained in the first 0.5 μm. For 800 K and 1000 K the D concentration is almost homogeneous throughout the whole damaged zone in both cases, after the W/D-D exposure, still we took the mean D concentration obtained between 0.2 μm and 1.2 μm. We show additional data obtained on samples for the TEM analysis after the simultaneous W/D-D exposure. We obtained very much the same D depth profiles as the ones presented in Fig. 6b and the values were extracted in the same manner as described above.

The D concentrations obtained for the simultaneous W/D-D exposure with ions are larger for all temperatures compared with the sequential exposure. The concentration ratio between the two experiments changes drastically from one temperature to the other. This is different compared with the experiment with atoms [6] where the ratio of D concentration for the simultaneous and sequential case was similar for all temperatures being about 1.3. For the ions there is a ratio of 2.1 in D concentration between simultaneous W/D-D and sequential W-D ion exposure at 450 K. The

difference in maximum D concentration decreases with the increase of the temperature to a factor of 1.7 at 600 K and 1.1 at 800 K. The decrease with the temperature up to 800 K implies that the presence of D atoms in the matrix is less efficient at higher temperatures. Whether this is due to the lower concentration in the W lattice – the so-called solute concentration - or due to the lower concentration of trapped D we cannot infer from the present experiment. Surprisingly, at 1000 K we again get an increase in the ratio to 2.1 between simultaneous and sequential experiment.

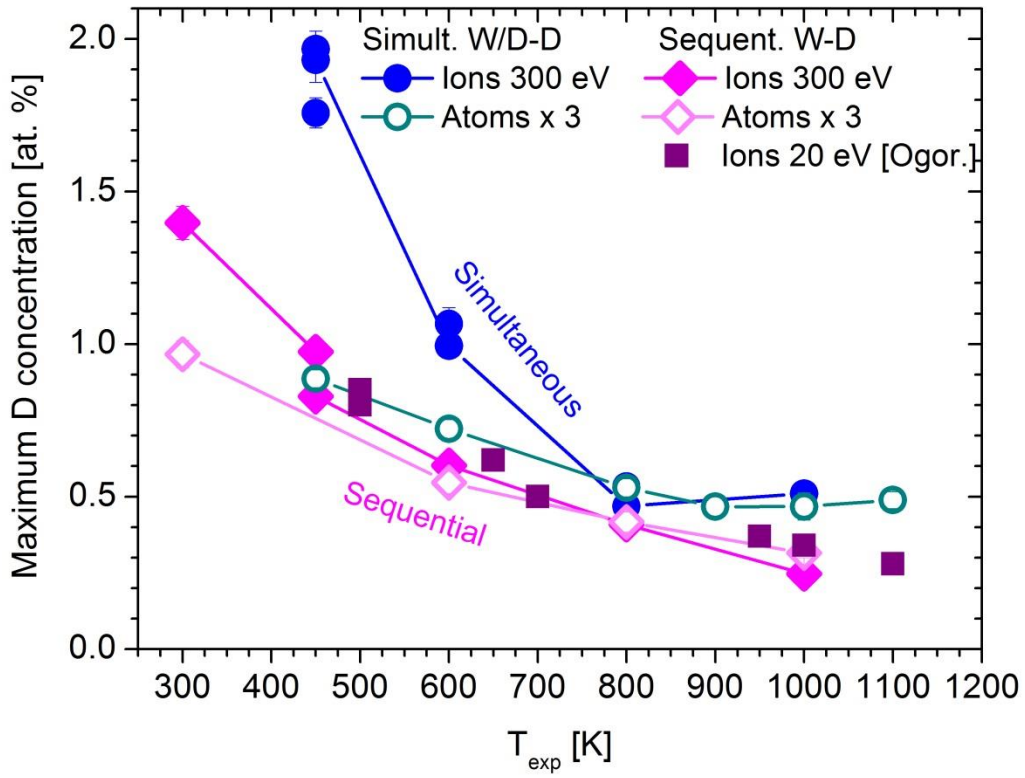

Figure 12: Maximum D concentration for the sequential W-D exposure and simultaneous W/D-D exposure. For comparison we also show the data for sequential and simultaneous results obtained by D-atom exposure [6] *multiplied by a factor of 3. The data from Ogorodnikova et al.* [32] *are also added for comparison, where a sequential experiment was performed with plasma exposure, ion energy of 20 eV/D at 470 K.*

We also show in Fig. 12 D concentration obtained with sequential W-D exposure with D atoms [6]. A direct quantitative comparison is not possible because as the atom exposure was done at 600 K instead of 450 K as for the ion case. However, by multiplying the atom data by a factor of three the maximum D concentration for the sequential exposures with D ions and D atoms show the same trend with increasing W irradiation temperature.

This difference is nicely depicted in figure 13 where a comparison between the TDS spectra of two atom and ion-exposed samples is shown. Both samples were W-ion-irradiated at 300 K. One was exposed to 300 eV D ions at 450 K (also shown in figure 8) and one exposed to D atoms with

0.28 eV/D energy at 600 K. For the atom case the TDS was taken from [25], where the heating ramp was the same as in the present ion case. The D desorption signals are normalized to the exposed surface area in order to be able to make the comparison. In the ion case we see two broad peaks (blue data points). One peak has a maximum at 600 K and a second, less intense one peaks at 780 K. In the atom case we see only one desorption peak with a maximum at around 800 K (red data points). We see that the decreasing slopes at high temperature coincide for the two spectra. However, in the atom case the low temperature peak is missing and the high temperature peak height is half of the ion's. This means that in the experiment presented here with D ion exposure, we can populate also the low-temperature traps, which ends up with about three times higher D total retention. This allowed us also to study the low-temperature defect evolution with the presence of D. We want to stress that the two peaks do not necessarily mean that there are only two types of defects or two single de-trapping energies involved. On the contrary, the shape of the TDS spectrum is a consequence of the sum of a multitude of different defects with different de-trapping energies. In figure 13 the results of a rate equation modelling of the measured TDS spectrum, using the MHIMS code [7], together with the corresponding de-trapping energies are shown. Five different de-trapping energies from 1.35 eV to 2.09 eV are necessary to describe the present TDS spectrum. A detailed modelling of the measured TDS spectra together with the corresponding depth profiles is beyond the scope of this publication and will be described in [35].

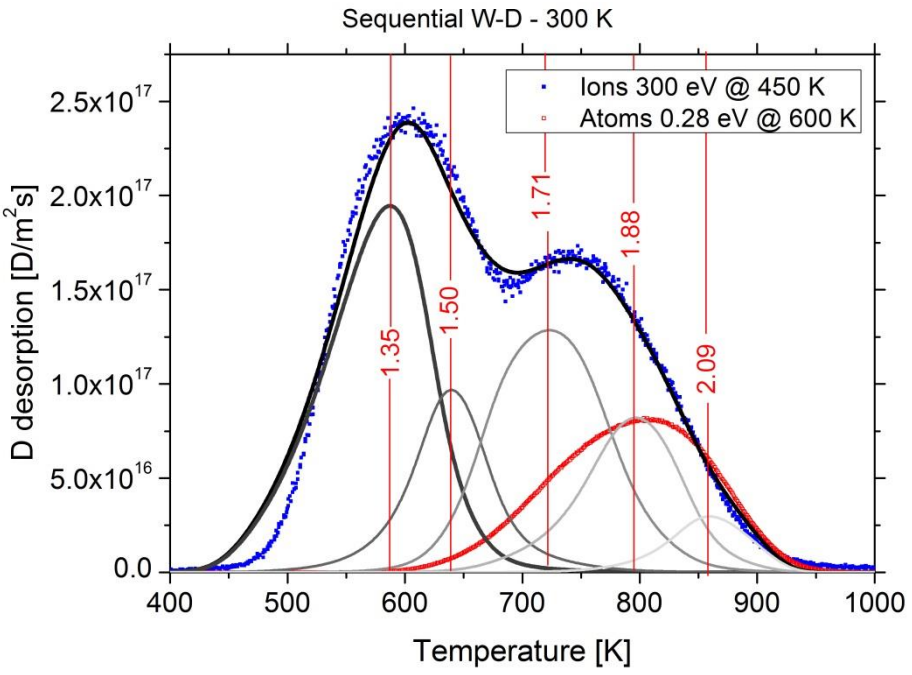

Fig. 13: Thermal desorption spectra for samples damaged at 300 K. Comparison between D ion exposure with energy of 300 eV/D at 450 K (blue dots) and D atom exposure with energy of 0.28 eV at 600 K from (red dots) [25]. *The thin grey lines are the results of a rate equation modelling of the measured TDS spectrum with the corresponding de-trapping energies. The heating ramp was 3 K/min.*

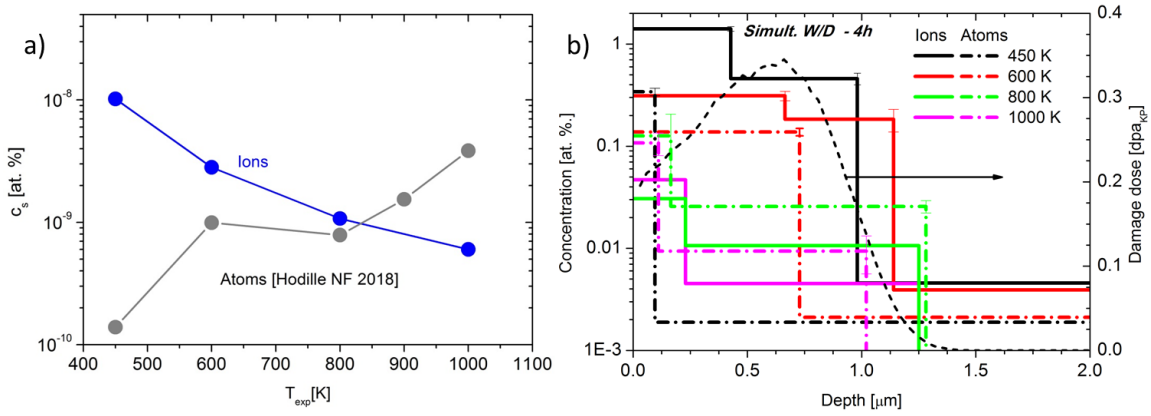

Figure 14: a) Solute D concentration for exposure to ions of 300 eV energy at 450 K and ion flux 2×10^{18} D/m^{2}s calculated according to equation (1) and exposure to atoms of 0.28 eV energy at 600 K and flux 5.4×10^{18} D/m^{2}s as calculated in [7]. *b) D depth profiles obtained after 4h of simultaneous W/D exposures, shown both for the D ion exposure and D atom exposure case.*

Comparing now the different procedures shown in figure 12 two main observations are obvious. For the simultaneous W/D-D exposures the D concentrations for ions show the same trend as in the atom case between 800 K and 1000 K. But a big difference can be observed for experiments at 450 K and 600 K, where the simultaneous D concentration for ions show a much larger effect of defect stabilization as compared with atoms. One possible explanation for the observed results and the difference between atom and ion exposure is based on the different concentrations c_S of solute D for these two cases. Figure 14a shows calculations of maximal c_S for the undisturbed lattice. For ions c_S can be calculated for steady state as [36, 37]:

$$c_S = \frac{(1-R)\, d\, \Gamma}{D\, \delta_W}, \qquad (1)$$

where R is the reflection coefficient, Γ is the ion flux, d is the average ion range, D is the diffusion constant and δ_W is the tungsten volume density. Figure 14a shows the dependence of c_S on temperature for R=0.5, d=5 nm for 300 eV/D ion energy, Γ=1.9×10^{18} D/m^{2}s and D=1.34×10^{-7} exp(0.2/k$_B$T) as calculated by DFT [10]. For these parameters the solute concentration for ions c_S decreases with the increase of temperature due to the increase of diffusivity. For D atom exposure with an energy of 0.28 eV and a flux of 5.4×10^{18} D/cm^{2}s c_S is also shown in Fig 14a as calculated in [7]. At 450 K c_S is two orders of magnitude smaller than for the ion case. However, in contrast to the

ions it increases with temperature, since the surface barrier can be overcome more easily and hence there is a larger uptake into the bulk at higher temperatures. At 600 K there is only a factor of three in favor of ions and at 800 K the two concentrations are similar. Above 800 K the solute concentration is even higher for atoms as compared to ions for given parameters.

We believe that this difference in the solute concentration observed as a function of temperature influences the amount of trapped D obtained for the simultaneous W/D exposure with ions and atoms. A comparison is shown in Fig. 14b. Namely, for a given amount of traps the solute concentration determines how fast the traps will be filled in a given amount of time and consequently how fast will be the D transport through the damaged zone.

This is especially pronounced for 450 K and 600 K experiments, where the solute concentration is high for the D ion exposure. For this reason the created traps during W irradiation are efficiently populated and the front can move forward. On the contrary, in the case of 0.28 eV D atoms simultaneous W/D exposure the solute concentration is small since the atoms need to overcome the barrier between the surface and bulk and they hardly populate near surface region in the case of 450 K. Depth profiles are shown in Fig. 14b for comparison. At 600 K the probability for atoms to overcome the barrier is larger. Therefore, for the atom experiment D penetrated 0.7 μm deep and the trapped D concentration is only two times lower compared with the D concentration after the W/D simultaneous experiment with ions, also shown in Fig. 14b.

To quantify the effect of D presence on defect stabilization we now compare the final D concentration after the simultaneous W/D-D exposure at 450 K (Fig. 12). The D concentrations obtained with ions are well above the results for atoms since there was a significant D trapping during the simultaneous W/D in the ion case. One can even observe that the simultaneous data for the atoms at 450 K match well with the sequential data for ions. We can conclude from this that no effect was observed in the atom case at 450 K due to the shallow penetration depth (Fig. 14b) which was also the conclusion from modeling the atom data in [7]. Therefore, high concentration of mobile atoms increases the speed of filling of the available traps and consequently increases stabilization of the defects.

At 600 K the maximum D concentrations after simultaneous W/D-D are in the ion as well as in the atom case above the sequential data since in both cases D was present and trapped during the W/D exposure. However, since the trapped D concentration during W/D exposure (Fig. 14a) was higher in the ion case we also get higher D concentration after the additional D exposure (Fig. 12). From this observation we conclude that the higher the concentration of the D is during the simultaneous W/D exposure the larger is the stabilization of the defects due to D presence.

During the simultaneous W/D exposure at higher temperatures (800 K and 1000 K) D is present throughout the whole W damaging zone in both cases, Fig. 14b. The concentrations of the solute D

and trapped D are even higher for the atom simultaneous case, as shown in figures 14a and 14b, respectively. However, overall the D concentrations are low due to high thermal de-trapping from the traps, being few 0.01 at.% and few 0.001 at.% for 800 K and 1000 K, respectively. The final D concentration values after the additional D exposures are similar for both cases (Fig. 12). At such high exposure temperatures only the high energy traps are populated by deuterium for our exposure conditions (Fig. 13). Therefore, one can speculate that because of small D concentrations during W/D exposure the differences between ion and atom case after the additional D exposure are small and in both cases we see a higher D defect stabilization at 1000 K as compared to 800 K, despite the lower D concentration. This leads us to believe that the mechanism of stabilization is somehow different at such high temperatures than at temperatures ≤ 800 K. On possible explanation is that defects start to agglomerate between 800 K and 1000 K (vacancies forming clusters), so maybe there is a transition and a new type of defect is being created by agglomeration, as was already speculated in [7]. In this case, D atoms would still populate such defect and contribute to the effect. Overall, from this comparison of simultaneous W/D-ion or -atom exposure one can conclude that the effect of the presence of D either trapped in the defects or in solute is clearly observed.

There is also a clear effect on the damage evolution when comparing the TDS spectra, shown in Fig. 8. Namely, when damage was performed at higher temperatures either for the sequential W-D or simultaneous W/D-D case, we almost observe a merging of the two peaks to one peak at 800 K. From our previous studies with atoms [8] we attributed the high temperature peak with a maximum at around 800 K to vacancy clusters of different size and cavities [7]. We did not observe the low-temperature peak as the exposure at 600 K does not allow the population of this peak. Now we see also the behavior of the low-temperature peak at 580 K which is typically attributed to vacancies with several levels of hydrogen atom occupation [7]. The discussion and TDS peak evaluation with rate equation models will be published in a separate paper where a model for defect stabilization will also be introduced [35].

We can imply that by comparing the TDS spectra and the ratios between the peaks the presence of D affects the defect stabilization, by D being trapped at the individual defect, as suggested by theory [4]. Namely, the exposure to ions at 450 K populates also the low-energy traps and indeed there is an increase of the ratio between simultaneous and sequential TDS peaks for the low-temperature peak. We get a ratio of 1.8 for the low-temperature peak as compared to the high-temperature peak getting a ratio of 1.5. The differences between the peak heights are higher in the 450 K case as compared to the 600 K data. In the case of 600 K both peaks have the same ratio of 1.3 between simultaneous and sequential data. We can deduce that the higher the trapped D concentration is during the simultaneous W/D exposure, the larger is the final stabilization also for the individual traps.

The TEM analysis on samples from the simultaneous W/D-D from Fig. 10 shows a different trend as compared with the maximum D concentrations or total D amounts shown in figures 12 and 9, respectively. While in the last case we observe a large difference for both NRA and TDS data for damaging temperatures between 450 K and 800 K there is hardly any difference in the dislocation densities from TEM images in that temperature range. This is an indication that the retention is not dominanted by dislocations even at exposure temperatures of 450 K but rather by vacancies, vacancy clusters and cavities as implied above from the TDS spectra. However, we see a trend in the defect structure obtaining long dislocation lines and tangles with a uniform distribution at 450 K and becoming shorter and having no tangles with the increase of the temperature.

Recently an experiment was performed where a second damaging at 300 K was done on an already damaged and D-populated sample [28]. An increase in D retention by a factor of two was observed similar to the one observed in our present simultaneous W/D-D exposure at 450 K. Experiments were interpreted such that D atoms get de-trapped and get mobile due to kinetic de-trapping and this causes new traps to be created during the second damaging with the presence of D atoms in the matrix. Another possible explanation for creation of additional damage during the second damaging is that the damage that would annihilate within the damage cascade with the already present damage in the sample without D does not annihilate since the defects are occupied by trapped D atoms. Neither from the results presented in [28] nor from the present experimental results we cannot unambiguously decide which of the two explanations apply. However, based on the present results we believe that stabilization of defects due to trapped D is more probable. It is important to note that this increased retention is a significant issue since till now it was shown that D retention in displacement-damaged W saturates at low damage levels of 0.2 dpa (corresponding to fluence of 7×10^{13} W/m^2 for damaging by 20 MeV ions [2, 31, 38] for 300 K damaging temperature) and will anneal to a large extent at divertor relevant temperatures of 1300 K [27, 29]. However, when D is present during the displacement damage, a significant fraction of the defects remain. Diffusion trapping modelling of the experiments shown here are presently under way to possibly isolate the underlying process and be able to extrapolate to reactor-relevant conditions.

3. Conclusions

We have studied the effect of the presence of D on defect production by high-energy W ions. For this we have performed a set of experiments where in one case samples were sequentially and in the other case simultaneously W ion irradiated and exposed to D ions at different temperatures. From the sequential series we have observed a reduction of D retention by 82% for W irradiation between 300 K and 1000 K. We have concluded that annealing of the defects after damaging at room temperature

and creating the defects at the same temperatures will neither give the same final defect structure nor yield to the same D retention.

By comparing the D depth profiles and thermal desorption spectra for sequential W-D and simultaneous W/D-D exposures we saw a clear effect of increase of defects that can trap D especially at 450 K and 600 K. Namely, we observe a factor of two increase in D concentration and in total D amount for the simultaneous W/D-D experiment as compared with the sequential W-D experiment at 450 K and a factor of 1.5-1.6 at 600 K. The temperature dependence of D-stabilized defects is very much dependent on the concentration of trapped D during the simultaneous experiment and for this reason the largest effect is at low temperature and should decrease with increasing temperature. From the comparison of the measured D concentration after the simultaneous W/D exposure one could imply that there is a limiting lower level of trapped D or solute D concentration that still affects the defects and below that value defects are not affected anymore by the presence of hydrogen. At 1000 K the difference between simultaneous and sequential case increases again. Clarifying the reason for this increase at 1000 K calls for additional experiments. TDS gave no indication that different trap types might have been created for the two different damaging series but gave us the information how the presence of D affects individual defects. In both cases, sequential and simultaneous, we have obtained two distinct D desorption peaks where the low-temperature peak is the highest for 450 K and 600 K experiments. The low-temperature peak is usually attributed to vacancies with different hydrogen atom occupancy [10, 39] meaning it is even more affected by the presence of D as compared to vacancy clusters to which we attribute the high temperature peak [7, 40]. For damaging at 800 K the two desorption peaks become of the same height.

The mean or maximum D concentrations extracted from the D depth profiles can be used as a measure for defect creation due to neutron irradiation in larger depths. These data are especially important to extrapolate to tritium transport, retention and permeation for future fusion reactors such as DEMO, where a damage level of several dpas per year are anticipated [41]. Surface temperatures of the components will be high: depending on the actual design and cooling option up to 800 K for the first wall and 1000 K and more in the divertor [42]. One could conclude from our data that D retention will be low due to thermal D de-trapping from the displacement damage created by neutron irradiation at high temperatures. However, four to six orders of magnitude higher fluxes [43] are expected in ITER as compared to the D flux of 10^{-18} D/m^{2}s in the present study. This high flux will lead to significant defect population even at higher temperatures and inherently larger stabilization of defects and larger hydrogen isotope retention also at higher temperatures. Moreover, in the bulk of the components in a DEMO reactor the temperature will decrease towards the cooling channels finally reaching the temperature of the cooling medium. To model tritium retention and permeation it is therefore important also to understand mechanisms at lower temperatures. We have shown that the

defect stabilization due to presence of D during damaging is most prominent when D concentration of trapped particles is high due to low thermal de-trapping from the defects.

Acknowledgement

This work has been carried out within the framework of the EUROfusion Consortium and has received funding from the Euratom research and training program 2014-2018 and 2019-2020 under grant agreement No 633053. Work was performed under EUROfusion WP PFC. The Polish authors also acknowledge the financial support from the Polish Ministry of Science and Higher Education, grant no. 3987/H2020-Euratom/2018/2/. The views and opinions expressed herein do not necessarily reflect those of the European Commission.

References

[1] W. R. Wampler and R. P. Doerner, "The influence of displacement damage on deuterium retention in tungsten exposed to plasma," *Nuclear Fusion,* vol. 49, p. 115023, 2009.

[2] O. V. Ogorodnikova and V. Gann, "Simulation of neutron-induced damage in tungsten by irradiation with energetic self-ions," *Journal of Nuclear Materials,* vol. 460, p. 60, 2015.

[3] S. C. Middleburgh, R. E. Voskoboinikov, M. Guenett and D. Riley, "Hydrogen induced vacancy formation in tungste," *J. Nucl. Mater.,* vol. 448, p. 270–275, 2014.

[4] D. Kato, H. Iwakiri , Y. Watanabe, K. Morishita and T. Muroga, "Super-saturated hydrogen effects on radiation damages in tungsten under the high-flux divertor plasma irradiation," *Nucl. Fusion,* vol. 55, p. 083019, 2015.

[5] P. Hautojärvi, H. Huomo, M. Puska and A. Vehanen, "Vacancy recovery and vacancy-hydrogen interaction in niobium and tantalum studied by positrons," *Phys. Rev. B,* vol. 32, no. 7, pp. 4326-4331, 1985.

[6] S. Markelj, T. Schwarz_Selinger, A. Zaloznik, M. Kelemen, P. Vavpetic, P. Pelicon, E. Hodille and C. Grisolia, "Deuterium retention in tungsten simultaneously damaged by high energy W ions and loaded by D atoms," *Nucl. Mater. Energ.,* vol. 12, pp. 169-174, 2017.

[7] E. Hodille, S. Markelj, T. Schwarz-Selinger, A. Zaloznik, M. Pecovnik, M. Kelemen and C. Grisolia, "Stabilization of defects by the presence of hydrogen in tungsten: simultaneous W-ion damaging and D-atom exposure," *Nucl. Fusion,* vol. 59, p. 016011, 2019.

[8] E. A. Hodille, A. Založnik, S. Markelj, T. Schwarz-Selinger, C. S. Becquart, R. Bisson and C. Grisolia, "Simulations of atomic deuterium exposure in self-damaged tungsten," *Nucl. Fusion,* vol. 57, p. 056002, 2017.

[9] A. Zaloznik, S. Markelj, T. Schwarz-Selinger and K. Schmid, "Deuterium atom loading of self-damaged tungsten at different sample temperatures," *J. Nucl. Mater.,* vol. 496, pp. 1-8, 2017.

[10] N. Fernandez, Y. Ferro and D. Kato, "Hydrogen diffusion and vacancies formation in tungsten: Density Functional Theory calculations and statistical models," *Acta Mater. ,* vol. 94, pp. 307-318, 2015.

[11] S. Markelj, A. Založnik, T. Schwarz-Selinger, O. V. Ogorodnikova, P. Vavpetič, P. Pelicon and I.

Čadež, "In situ NRA study of hydrogen isotope exchange in self-ion damaged tungsten exposed to neutral atoms," *Journal of Nuclear Materials,* vol. 469, p. 133–144, 2016.

[12] I. Bizyukov and . K. Krieger, "Dual Beam Experiment for Simultaneous Irradiation of Surfaces with Ion Species of Gaseous and Solid-State Elements," *Rev. Sci. Instr.,* vol. 77, p. 043501, 2006.

[13] e. H. Ullmaier, Landolt-Börnstein – Group III Condensed Matter. Volume 25: "Atomic Defects in Metals", Berlin Heidelberg: Springer-Verlag , 1991.

[14] ASTM Int'l E521-16, "Standard practice for neutron radiation damage simulation by charge-particle irradiation," in *Annual Book of ASTM Standards vol 12.02*, Philadelphia, PA, American Society for Testing and Materials, 2016, p. p 8.

[15] M. Balden and J. Roth, "New Weight-Loss Measurements of the Chemical Erosion Yields of Carbon Materials under Hydrogen Ion Bombardment," *J. Nucl. Mater.,* vol. 280, p. 39, 2000.

[16] T. Schwarz-Selinger, A. Von Keudell and W. Jacob, "Novel method for absolute quantification of the flux and angular distribution of a radical source for atomic hydrogen," *Journal of Vacuum Science & Technology A: Vacuum, Surfaces, and Films,* vol. 18, p. 995–1001, 2000.

[17] M. E. Bouanani, P. Pelicon, A. Razpet, I. Cadez, M. Budnar, J. Simcic and S. Markelj, *Nucl. Inst. Meth. Phys. Res. B,* vol. 243, p. 392, 2005.

[18] J. Ziegler, "www.srim.org.," [Online].

[19] T. Schwarz-Selinger, "Deuterium Retention in MeV Self-Implanted Tungsten: Influence of Damaging Dose Rate," *Nuclear Energy and Materials,* vol. 12, p. 683–688 , 2017.

[20] M. Meyer, "SIMNRA User's Guide, Report IPP 9/113," Max-Planck-Instutut für Plasmaphysik, Garching, Germany, 1997. [Online]. Available: http://www.rzg.mpg.de/~mam/.

[21] K. Schmid and U. von Toussaint, *Nucl. Instr. and Meth. in Phys. Res. B,* vol. 281, p. 64, 2012.

[22] B. Wielunska, M. Mayer, T. Schwarz-Selinger, U. von Toussaint and J. Bauer, "Cross Section Data for the D(3He,p)4He Nuclear Reaction from 0.25 to 6MeV," *Nuclear Instruments and Methods in Physics Research Section B: Beam Interactions with Materials and Aanlysis,* vol. 371, p. 61, 2016.

[23] W. Möller and F. Besenbacher, "A Note on the 3He+ D Nuclear-Reaction Cross Section," *Nuclear Instruments and Methods,* vol. 168, p. 111, 1980.

[24] E. Salançon, T. Dürbeck, Schwarz-Selinger, F. Genoese and W. Jacob, *J. Nucl. Mater.,* vol. 376, p. 160, 2008.

[25] M. Pečovnik, S. Markelj, A. Založnik and T. Schwarz-Selinger, "Influence of grain size on deuterium transport and retention in self-damaged tungsten," *J. Nucl. Mater.,* vol. 513, p. 198, 2019.

[26] P. Wang, W. Jacob, L. Gao, T. Dürbeck and T. Schwarz-Selinger, "Comparing deuterium retention in tungsten films measured by temperature programmed desorption and nuclear reaction analysis," *Nuclear Instruments and Methods in Physics Research Section B: ,* vol. 30, pp. 54-61, 2013.

[27] A. Založnik, S. Markelj, T. Schwarz-Selinger, Ł. Ciupiński, J. Grzonka, V. P. and P. Pelicon, "The influence of the annealing temperature on deuterium retention in self-damaged tungsten," *Phys. Scr.,* vol. T167, p. 014031, 2016.

[28] Schwarz-Selinger, T., Bauer, J., Elgeti, S. and S. Markelj, "Influence of the presence of deuterium on displacement damage in tungsten," *Nucl. Materials and Energy,* vol. 17, p. 228–234, 2018.

[29] E. Markina, M. Mayer, A. Manhard and T. Schwarz-Selinger, "Recovery temperatures of defects in tungsten created by self-implantation," *J. Nucl.r Mater.,* vol. 463, pp. 329-332, 2015.

[30] S. Markelj, O. V. Ogorodnikova, P. Pelicon, T. Schwarz-Selinger and I. Cadez, "Temperature dependence of D atom adsorption on polycrystalline tungsten," *Appl. Surf. Sci. ,* vol. 282, pp. 478-486, 2013.

[31] M. H. J. 't Hoen, B. Tyburska-Püschel, K. Ertl, M. Mayer, J. Rapp, A. W. Kleyn and P. A. Zeijmans

van Emmichoven, "Saturation of deuterium retention in self-damaged tungsten exposed to high-flux plasmas," *Nucl. fusion 52,* p. 023008, 2012.

[32] O. V. Ogorodnikova, Y. Gasparyan, V. Efimov, Ł. Ciupiński and J. Grzonka, "Annealing of radiation-induced damage in tungsten under and after irradiation with 20 MeV self-ions," *Journal of Nuclear Materials,* vol. 451, no. 1-3, pp. 379-386, 2014.

[33] G.-Y. Huang, N. Juslin and B. D. Wirth, "First-principles study of vacancy, interstitial, noble gas atom interstitial and vacancy clusters in bcc-W," *Computational Materials Science,* vol. 123, p. 121–130, 2016.

[34] Simmonds, M.J., Wang, Y.Q., Barton, J.L., M. Baldwin, Yu, J.H., Doerner, R.P. and Tynan, G.R., "Reduced deuterium retention in simultaneously damaged and annealed tungsten," *J. Nucl. Mater.,* vol. 494, p. 67, 2017.

[35] M. Pečovnik, S. Markelj, E. Hodille, T. Schwarz-Selinger and C. Grisolia, "Sinergistic effect between D and W irradiation in damage creation in tungsten," *private communication.*

[36] E. A. Hodille, N. Fernandez, Z. A. Piazza, M. Ajmalghan and Y. Ferro, "Hydrogen supersaturated layers in H/D plasma-loaded tungsten: A global model based on thermodynamics, kinetics and density function theory data," *Phys. Rev. Mater. 2,* p. 093802, 2018.

[37] L. Gao, W. Jacob, U. von Toussaint, A. Manhard, M. Balden, K. Schmid and T. Schwarz-Selinger, "Deuterium supersaturation in low-energy plasma-loaded tungsten surfaces," *Nucl. Fusion,* vol. 57, p. 016026, 2017.

[38] V. Alimov, Y. Hatano, B. Tyburska-Püschel, K. Sugiyama, I. Takagi, Y. Furuta, J. Dorner, M. Fußeder, K. Isobe, T. Yamanishi and M. Matsuyama, "Deuterium retention in tungsten damaged with W ions to various damage levels," *Journal of Nuclear Materials,* vol. 441, p. 280–285, 2013.

[39] D. F. Johnson and E. A. Carter, "Hydrogen in tungsten: Absorption, diffusion, vacancy trapping, and decohesion," *J. Mater. Res.,* vol. 25, no. 2, p. 315, 2010.

[40] O. V. Ogorodnikova, "Fundamental aspects of deuterium retention in tungsten at high flux plasma exposure," *J. Appl. Phys. ,* vol. 118, p. 074902, 2015.

[41] J.-H.You, "A review on two previous divertor target concepts for DEMO: mutual impact between structural design requirements and materials performance," *Nucl. Fusion,* vol. 55, no. . , (2015)., p. 113026, 2015.

[42] M. e. a. Rieth, "Recent progress in research on tungsten materials for nuclear fusion applications in Europe," *J. Nucl. Mater.,* vol. 432, p. 482–500, 2013.

[43] J. Roth, E. Tsitrone, A. Loarte, T. Loarer, R. Neu, V. Philipps and S. Brezinsek, "Recent analysis of key plasma wall interactions issues for ITER," *Journal of Nuclear Materials,* vol. 390–391, no. 1., p. 1–9, 2009.